Publishing House
AKAPIT

COMPUTER METHODS IN MATERIALS SCIENCE

Informatyka w Technologii Materiałów

Vol. 11, 2011, No. 2

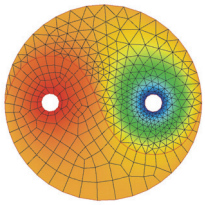

OPTIMISATION OF PARAMETERS OF SINGLE CRYSTAL MODEL FOR ALUMINIUM BICRYSTALS

WOJCIECH WAJDA*, HENRYK PAUL

Instytut Metalurgii i Inżynierii Materiałowej PAN, Reymonta 25, 30-059 Kraków, Poland
**Corresponding author: nmwajda@imim-pan.krakow.pl*

Abstract

The single crystal plasticity model is commonly used to simulate single- and bicrystal material behaviour. However the parameters for the model are difficult to find in the literature. In the paper inverse technique was used to obtain the parameters. Obtained parameters were applied to simulate behaviour of the plain strain compressed bicrystal. The results were validated by experiment.

The experimental part (for validation purpose) focused on local orientation changes during plain strain compression of different aluminium bicrystals. Bicrystals composed of cube/hard {100)<001>/{110}<011> and cube/Goss {100}<001>/{110}<001> oriented grains were chosen. In both cases/configurations, the grains boundaries were parallel to compression planes. The analysis of the deformed samples was carried out at various scales by means of optical and scanning electron microscopy.

Key words: aluminium, bicrystal, cube, hard, Goss orientations, crystal plasticity model

1. INTRODUCTION

The most common case of metal forming is the formation of a polycrystalline aggregate. However, in an experimental approach, it is difficult to analyse deformed polycrystalline aggregate, especially when it comes to the investigation of a very fundamental mechanism of deformation, namely slip and lattice rotation. Analysis of deformed single or bicrystal allows to investigate mechanisms of deformation in "controlled conditions". To support the analysis with numerical simulation proper model and the parameter are required.

In the paper the optimization of the single crystal plasticity model parameters was done. The parameters were obtained for single crystal of aluminium with cube {100)<001> orientation compressed in plane stress conditions. The flow stress obtained form experiment was used to construct goal function for inverse analysis. Validation of obtained parameters focused on proper determination of crystallographic mechanisms of deformation. In order to analyse influence of orientation changes on model predictions the validation was carried out for aluminium bicrystal deformed in plane strain conditions.

The optimisation of parameters is made for single crystal plasticity model developed by Huang (1991).

In order to obtain experimental data for validation the aluminium bicrystal with cube {100)<001> and hard {110}<011> as well as cube {100)<001> and Goss {110}<001> grains were plain stress compressed. ({hkl}<uvw> signify the compression plane of normal ND and the elongation direction ED, respectively). The grains boundary was positioned parallel to the compression plane. Both hard {110}<011> and Goss {110}<001> crystallites

 ISSN 1641-8581

show stable behavior during deformation. However, the crystallite strength is much higher when a grain is in hard orientation. The strength of Goss and cube oriented crystallites is comparable.

In the experiment, particular interest is focused on the changes of local lattice orientation during deformation. Various investigation techniques were used, including optical and scanning electron microscopy.

In this paper, the authors assume on the basis of (Paul and Driver,2005; Paul et at., 2006) that only easy glide slip systems can operate during deformation. Consequently, the deformation bands developed due to local lattice rotation. The goal regarding crystal plasticity model is to develop method of obtaining material parameters and evaluate model capability of predicting local lattice rotation.

2. EXPERIMENTAL AND ANALYSIS PROCEDURES

A bicrystal with controlled orientations was grown from high purity Al (99.998%) by a modified Bridgman technique (horizontal solidification), using split graphite moulds. The dimensions of the bicrystal bars were approximately 15 mm (thickness) x 22 mm (width) x 150 mm (length). Samples that were 15 mm high, 10 mm long and 10 mm wide were sectioned from a bar and plane strain compressed at a nominal strain rate of $\sim 10^{-4} s^{-1}$. Teflon films were used as a lubricant and periodically replaced at strain intervals of about 0.2. To favour deformation banding and reduce dynamic recovery effects, the tests were performed at 77 K by immersing the channel-die device in a reservoir with liquid nitrogen. This procedure gives, at relatively low strains, a work-hardened structure containing clearly defined bands.

The cube/hard {100}<001>/{110}<011> and cube/Goss {100)<001>/{110}<001> bicrystal configurations were used in channel-die compression test in order to study the influence of misorientation between grains on material hardening and strain localization. As mentioned before, the grain boundary was positioned parallel to the compression plane. The channel die test was carried out at the Laboratory of the Institute of Metallurgy and Material Science of the Polish Academy of Sciences.

2.1. Plane strain deformation analysis – experiment

The microstructures of material deformed were characterized over a wide range of scales using a combination of scanning electron microscopy (SEM) and optical metallography. The samples were sectioned in the ND-ED plane by wire cutting. For thin foil preparation, a twin set electropolishing technique was used in standard nitric acid–methanol solution. Optical microscopy investigation was carried out with polarized light on electropolished and slightly anodized (in 2% fluoroboric acid solution) sections. The majority of metallographic observations were made on the longitudinal plane, i.e. ND-ED. The orientations of crystallites that constituted the bicrystals were checked by the X-ray back reflexion Laue method. The deformed specimens were mostly examined by scanning electron microscopy (SEM) in a JEOL JSM 6500F, equipped with a field emission gun (FEG) and electron backscattered diffraction (EBSD) facilities, in which microscope control, pattern acquisition and solution were performed with the HKL Channel 5TM system. Local orientation data, obtained by SEM/EBSD technique on the ND-ED section were transformed to the standard ED-TD (TD is the transverse direction) reference system and presented in the form of {111} pole figures.

2.2. Finite element simulation

A simplified approach to the simulation of bicrystal deformational behaviour was presented in (Wajda & Paul, 2009), where a different flow curve obtained in single crystal plain strain compression was used to describe mechanical properties of each crystallites. The approach is in accordance with the general assumption that aluminium bicrystals deformed up to medium strains behave to a large extent like two individual single crystals (Raabe et at., 2001). However, it does not take into account the crystallographic aspects of deformation. In this paper, the material model was described by means of a single crystal plasticity model. Combined with the previous approach, this allows one to take into consideration and analyse the contribution of each slip system to global deformation and lattice rotation. In the model, the plastic deformation occurs due to crystallographic dislocation slip. Deformation by diffusion, twinning and grain boundary sliding is not taken in to account in the model. The slip on a slip

system occurs solely due to acting resolved shear stress on the system. As described by Huang (1991), the total deformation gradient ($\boldsymbol{F}$) is composed from two elements: stretching and rotation ($\boldsymbol{F}^*$) and inelastic gradient ($\boldsymbol{F}^p$), as shown in equation (1).

$$\boldsymbol{F} = \boldsymbol{F}^* \cdot \boldsymbol{F}^p \tag{1}$$

Elastic properties are assumed to be unaffected by the slip. The stress in elastic domain is calculated based on gradient $\boldsymbol{F}^*$. The velocity gradient in the current state is decomposed into a symmetric rate of stretching ($\boldsymbol{D}$) and an antisymmetric spin tensor ($\boldsymbol{\Omega}$), which in turn can be decomposed (equation (2)) into a lattice part (superscript *) and a plastic part (superscript p).

$$\boldsymbol{D} = \boldsymbol{D}^* + \boldsymbol{D}^p, \quad \boldsymbol{\Omega} = \boldsymbol{\Omega}^* + \boldsymbol{\Omega}^p \tag{2}$$

The decomposition must satisfy the following conditions (equations (3)):

$$\boldsymbol{D}^* + \boldsymbol{\Omega}^* = \dot{\boldsymbol{F}}^* \cdot \boldsymbol{F}^{*-1}, \quad \boldsymbol{D}^p + \boldsymbol{\Omega}^p = \sum_{\alpha} \dot{\gamma}^{(\alpha)} \boldsymbol{s}^{*(\alpha)} \otimes \boldsymbol{m}^{*(\alpha)} \tag{3}$$

where: $\dot{\gamma}^{(\alpha)}$ is the slipping rate on slip system α, $\boldsymbol{s}^{*(\alpha)}$ and $\boldsymbol{m}^{*(\alpha)}$ are the slip direction and the normal to slip plane in the current configuration for slip system α, respectively.

Equations (4) are used to relate the slip direction and the normal to slip plane in the current and reference configuration.

$$s^{*(\alpha)} = F^* \cdot s^{(\alpha)}, \quad m^{*(\alpha)} = m^{(\alpha)} \cdot F^{*-1} \tag{4}$$

where: $s^{(\alpha)}$ and $m^{(\alpha)}$ are the slip direction and the normal to slip plane in reference configuration for slip system α, respectively.

The crystalline slip in the model is assumed to follow the Schmid's law. This implies the slip rate $\dot{\gamma}^{(\alpha)}$ on any slip system depends only on the Schmid stress ($\tau^{(\alpha)}$). The Schmid stress depends on the current stress state ($\boldsymbol{\sigma}$) and the current lattice orientation ($\boldsymbol{s}^{*(\alpha)}$, $\boldsymbol{m}^{*(\alpha)}$). It is expressed by the definition expressed in equation (5):

$$\tau^{(\alpha)} = \boldsymbol{m}^{*(\alpha)} \cdot \boldsymbol{\sigma} \cdot \boldsymbol{s}^{*(\alpha)} \tag{5}$$

The amount of shear on a slip system $\dot{\gamma}^{(\alpha)}$ is calculated based on the Schmid's law. For rate-dependent crystallite, it is determined by means of the following equation (6):

$$\dot{\gamma}^{(\alpha)} = \dot{a}^{(\alpha)} \frac{\tau^{(\alpha)}}{g^{(\alpha)}} \left| \frac{\tau^{(\alpha)}}{g^{(\alpha)}} \right|^{n-1} \tag{6}$$

where $\dot{a}^{(\alpha)}$ is the reference strain rate on slip system α, $g^{(\alpha)}$ is the current strength for slip system α and it is described by equation (7),

$$\dot{g}^{(\alpha)} = \sum_{\beta} h_{\alpha\beta} \dot{\gamma}^{(\beta)} \tag{7}$$

The $h_{\alpha\beta}$ is the matrix of hardening modules. It describes self-hardening and latent hardening of slip systems. The self-hardening module is given by the equation:

$$h_{\alpha\alpha} = h(\gamma) = h_0 \sec h^2 \left| \frac{h_o \gamma}{\tau_s - \tau_o} \right| \tag{8}$$

The latent module is related to the self-hardening module by coefficient q:

$$h_{\alpha\beta} = q h(\gamma), \quad \alpha \neq \beta \tag{9}$$

3. RESULTS

3.1. Plane strain compression test

The crystallites configuration of cube/Goss {100}<001>/{110}<001>-type represents the unstable vs. stable combination of grain orientations. In macro scale, the cube/Goss {100)<001>/{110}<001> bicrystal with boundary positioned parallel to the compression plane initially appears to undergo larger strains in the cube part (at 36% reduction), but the two zones even out at higher strains (69% reduction). A crystallite with the Goss orientation does not reveal the formation of band-like strain inhomogeneities. This behaviour is quite different from that of a cube crystallite which shows a strong tendency for strain localization from the early stages of deformation. The formation of band-like strain inhomogeneities in the unstable cube orientation increases greatly with deformation and their distribution in the sample section is highly inhomogeneous (figures 1a and b). They usually penetrate the whole volume of the grain, separating areas with large lattice rotation, but they do not show any tendency to intersect grain boundaries.

An example of microstructure analysed by local orientation measurements using SEMFEG/EBSD system is shown in figure 1b for the area comprising the grain boundary. The orientation maps for the cube/Goss {100)<001>/{110}<001> bicrystal show differences in the morphology of the formed strain inhomogeneities. In the case of the cube-oriented

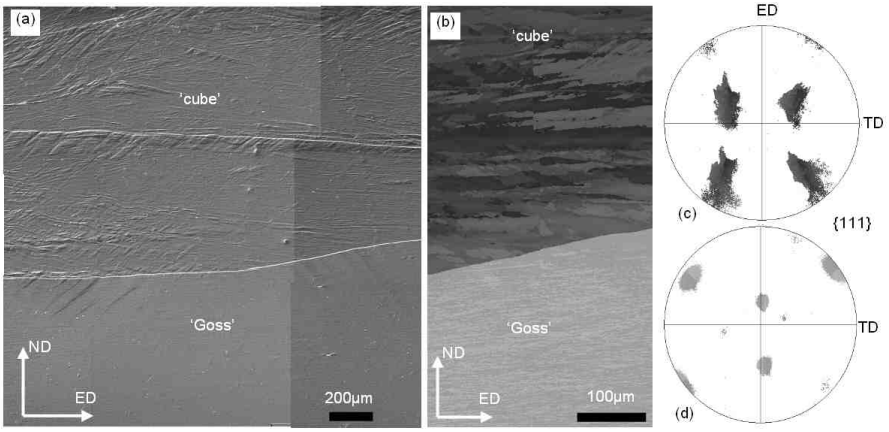

Fig. 1. *Stable vs. usntable behaviour of bicrystal deformed up to 68% with {100}<001>/{110}<001> grain orientations and grain boundary situated parallel to the compression plane. (a) Microstructure observed at the optical microscopy scale, (b) SEM-FEG/EBSD orientation map (in grey scale) and corresponding {111} pole figures: (c) cube-oriented crystallite, (d) Goss-oriented crystallite.*

grain, the crystal lattice undergoes major rotations, especially inside the elongated areas (figures 1a and b). This process leads finally to the formation of a coarse micro-band structure aligned approximately parallel to the compression plane. The crystallites with the Goss orientation demonstrate only a weak tendency for lattice rotation, occurring mainly around an axis close to ND (figure 1a and b). The {111} pole figures, shown in figure 1c and d (from particular crystallites) illustrate the tendency in the crystal lattice rotation. The cube oriented part shows the tendency to form band-like inhomogeneities of deformation. This leads to the occurrence of strong orientation changes. The created misorientation assumes most often the angular values of ~15^{o} (in some cases up to 35^{o}). Great disturbances of crystal lattice near grain boundary in a cube oriented crystallite are responsible for local displacement of the boundary or changes of its inclination. The structure of the crystallite with Goss orientation is definitely more homogeneous. It does not show a tendency to create any forms of localized strain. The majority of the boundaries are low-angle boundaries described by <2^{o} misorientation. The global tendency in the rotation of the initial crystal orientation results from the rotation about ND. It is especially well visible near the grain boundary.

The cube/hard {100)<100>/{110}<011> combination is very heterogeneous as the cube grain undergoes large strains, while the much harder {110}<011> orientation involves hardly any deformation. Visual inspection suggests that the softer cube grain undergoes strains that are up to twice the value of the global or nominal thickness reduction, while the harder grain is significantly less deformed.

As a result of the continuity requirement at the grain boundary, the cube grain tends to flow over the harder grain and eventually at 59% reduction almost wraps around it. In the latter case, there are large transition zones near the grain boundary that are described in more detail below. The formation of deformation bands in the cube grain are similar to those in cube/Goss {100}<001>/{110}<001> bicrystal. The hard grain in general remains stable. Only the zones at the ends of a specimen get deformed in order to accommodate the large deformation of the cube crystallite. The behaviour of the cube/hard {100)<001>/{110}<011> bicrystal is surprising in that a transition zone that is about 1.5 mm wide is developed from the initial hard orientation. This is shown in detail in figure 2a and is probably due to the very high-localized shear of the hard {110}<011> grain as it deforms near the cube {100)<001>. The volumes of the hard crystallite lying near the grain boundary must accommodate the incompatibilities between the neighbouring grains, leading to a strongly deformed (and elongated) cube grain and the slightly elongated hard crystallite. As shown in figure 2b, this induces a broad orientation spread across the grain boundary and the transition zone (near the free surfaces of the sample). The figure shows a strong, continuous dispersion of the {111} poles, characterized by strong scattering by (±)TD rotation with some additional rotations around the ED and ND axes. The misorientations calculated with respect to the first measured point lying within the cube grain across the grain boundary reflect the difference in the formed structure (figure 2c). There is only about 12–15^{o} between the hard grain and the first measured point in the cube grain as a result of the rapid rotation of the cube grain near the transition zone towards the {110}<011> orientation.

3.2. Inverse method and validation of FE simulation

The parameters for the model were obtained by inverse technique. The stress measured during the experiment was compared to the one calculated by means of the FE model. The stress was measured

during plane strain compression of a aluminium single crystal with cube orientation. The parameters of the single crystal model were changed according to the simplex optimisation method until the difference between the stresses was minimized. The obtained set of parameters was used for each orientation during the simulation of bicrystal deformation. The obtained parameters are presented in table 1. Because of long computation time, the q parameter was assumed equal 0.0 to reduce number of optimized parameters and calculation time. By setting q equal 0 the latent part (equation 9) was not taken into account in calculation. The q parameter has little effect on obtained stress, which was calculated in order to optimize other parameters.

node elements were used. The nominal rate of deformation was set as in experiment ($10^{-4}s^{-1}$).

Among many variables taken in to account by the crystal plasticity model, particularly the orientation changes (normals to slip planes and slip directions in current configuration) and total cumulative shear strain on all slip systems were investigated. The global pole figures were drawn based on the calculated normal vectors to slip planes. The simulation of plain strain compression test for each bicrystal was carried out up to 50% of deformation. By changing friction conditions, their influence on lattice orientation was investigated. The frictionless and low-friction conditions were applied during simulations.

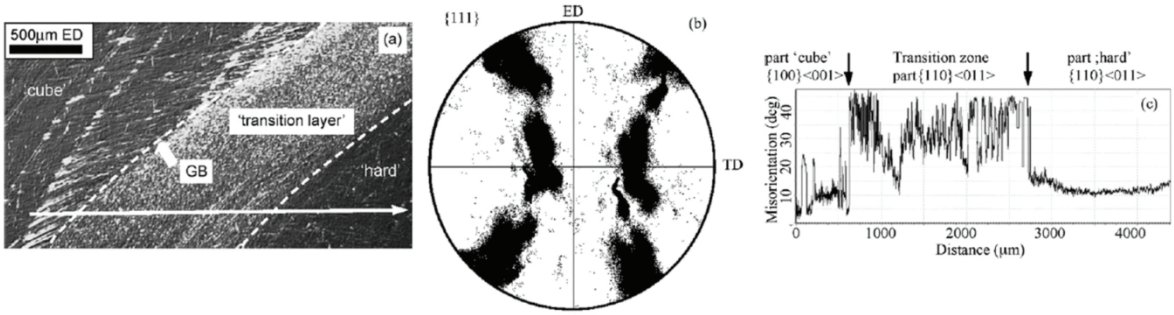

Fig. 2. *(a) Optical micrograph of the transition zone near the grain boundary in a 'cube/hard' bicrystal sample deformed to 59%. (b) {111} pole figure showing orientation changes across the grain boundary and transition zone (scan area of 200μm×5000μm). (c) Cumulative misorientation profile (with respect to the first point) lying within the 'cube' grain across the transition zone. SEM-FEG/EBSD measurements in the ND-ED plane with the step size of 200 nm.*

Table 1. *The parameters obtained by inverse technique for aluminium at the temperature of liquid nitrogen.*

Parameter	$\dot{a}$, s^{-1}	n, -	τ_0 , MPa	h_0, MPa	h_s, MPa	q, -	data fit error, %
Value	3,36E-005	1,866	125,87	59,4802	4,742	0.0	3,5

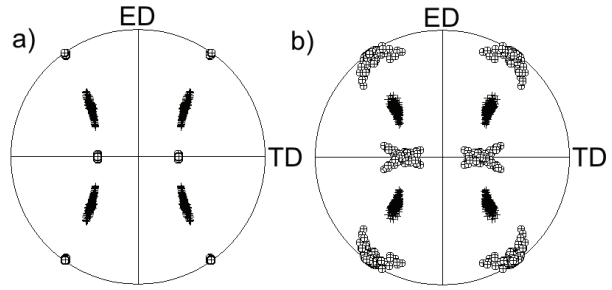

Fig. 3. *The {111} pole figures obtained from the FE simulation of cube/hard bicrystal plane strain compression. The simulations were carried out a) under frictionless conditions, and b) with a small friction coefficient equal to 0.05.*

Based on the obtained parameters the bicrystals compression were simulated. All simulations presented in this paper are three dimensional with the average element size 1 mm. The standard Abaqus 8

The calculated pole figures for cube/hard {100}<001>/{110}<011> bicrystal are presented in figure 3a and b. The pole figures allow one to conclude that the hard {110}<011> orientation is stable and the behaviour of the cube {100}<001> crystallite is unstable, particularly when there was no friction applied (figure 3a).

A small friction coefficient, equal 0.05, results in instable behaviour of hard {110}<011> oriented crystallite and small rotation around normal direction (ND) of cube {100}<001> crystallite. The rotation of the hard {110}<011> crystallite occurs mostly at the grain border at the ends of the specimen. In this region, the total cumulative shear strain is highest for the frictionless as well as low-friction conditions (figure 4a and b). This implies the highest activity of the slip system in this region. As it was shown in (Wajda & Paul, 2009), the rotation is needed to accommodate large deformation of cube {100}<001> crystallite. The region is consistent with experimentally obtained transition zone. It is also located in the hard crystallite as in the experiment.

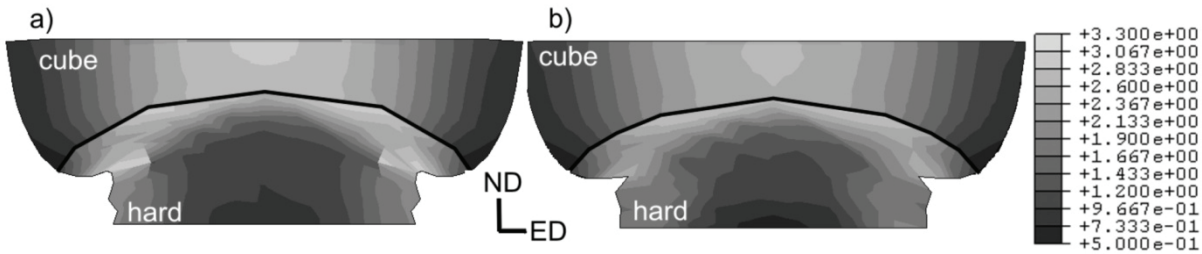

Fig. 4. *Distribution of the total cumulative shear strain in all slip systems obtained from the FE simulation of cube/hard bicrystal plane strain compression: a) without friction and b) with small friction coefficient equal to 0.05.*

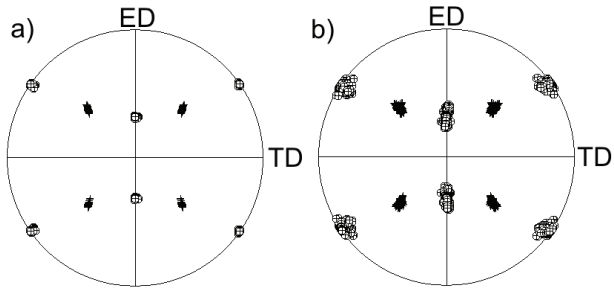

Fig. 5. *The {111} pole figures obtained from the FE simulation of cube/Goss bicrystal plane strain compression. The simulations were carried out a) under frictionless conditions, and b) with a small friction coefficient equal to 0.05.*

tions, the distribution of the total cumulative shear strain is almost uniform (figure 6a). For a small coefficient, higher values of total cumulative shear strain are observed in Goss {110}<001> bicrystal. This indicates a higher activity of slip systems (figure 6) in the case of higher friction.

4. CONCLUSIONS

Application of inverse analysis allows find parameters of the model. The calculated parameters allows to fit data (for cube orientation) with error

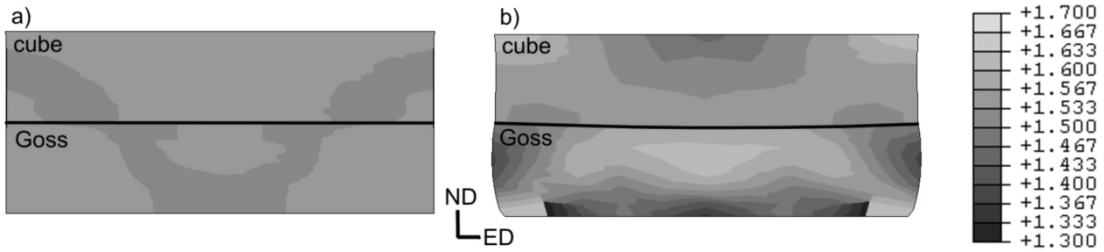

Fig. 6. *Distribution of the total cumulative shear strain in all slip systems obtained from the FE simulation of cube/Goss bicrystal plane strain compression a) without friction and b) with a small friction coefficient equal to 0.05.*

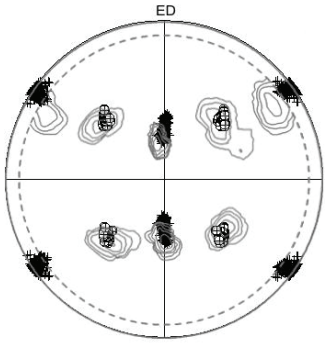

Fig. 7. *A comparison of the calculated and experimental textures of a deformed cube/Goss bicrystal. The continuous line shows the experimental texture. Bicrystal deformed up to 66%.*

The cube {100}<001> and Goss {011}<100> crystallites show similar hardening, so the deformation is more uniform than in the case of cube/hard {100}<001>/{110}<011> bicrystal. When the simulation was performed for low-friction conditions, the rotation around ND is observed (figure 5b), while in the case of frictionless conditions, the rotation does not appear (figure 5a). For the frictionless conditions, the distribution of the total cumulative shear strain is almost uniform (figure 6a). For a small coefficient, higher values of total cumulative shear strain are observed in Goss {110}<001> bicrystal. This indicates a higher activity of slip systems (figure 6) in the case of higher friction.

4. CONCLUSIONS

Application of inverse analysis allows find parameters of the model. The calculated parameters allows to fit data (for cube orientation) with error 3,5%. Calculated texture, local rotation and deformation distribution (cumulative shear) agree with experimental observations (figure 7). In addition, at the macro level, the calculated shape of the specimens as well as transition zones in cube/hard {100)<001>/{110}<011> bicrystal agree with experimental data. However, most probably due to relatively large finite element size, the model does not predict the deformation band observed in cube crystallite.

The results of FE simulations show an important influence of friction on obtained textures. Another factor which significantly influences the global texture development of cube crystallite is the orientation of the other crystallites and their strength. Hard crystallites - due to their resistance to deformation - enforce higher deformation of cube crystallite and its rotation.

The large finite element size was used in order to reduce computation time. This may have influenced

the obtained results. However, the calculated results are generally consistent with experimental data.

REFERENCES

Huang, J., 1991, A user material subroutine incorporating single crystal plasticity in the Abaqus finite element program, http://www.columbia.edu/~jk2079/fem/umat_documentation.pdf

Paul, H., Driver, J.H., 2005, Deformation behaviour of channel-die compressed Al bicrystals with {100}<001>/{110}<001> orientation, *Arch. Metal. Mater*., 50, 209-218.

Paul, H., Driver, J.H., Maurice, C., Bijak, M., 2006, Large strain Deformation substructures and local crystallography in {100}<001>/{110}/<001> aluminium bicrystals, *Arch. Metal. Mater*., 51, 43-53.

Raabe, D., Sachtleber, M., Zhao, Z., Roters, F., Zaefferer, S., 2001, Micromechanical and macromechanical effects in grain scale polycrystal plasticity experimentation and simulation, *Acta Mater*., 49, 3433-3441.

Wajda, W., Paul, H., 2009, Modeling of microstructure and texture evolution of channel-die deformed aluminum bicrystals with {100}<001>/{110}<011> grains orientation, *Comput. Methods Mater. Sci*., 9, 277-282.

OPTYMALIZACJA I WERYFIKACJA PARAMETRÓW MODELU 'CRISTAL PLASTICITY' DLA BIKRYSZTAŁÓW ALUMINIUM

Streszczenie

Implementacja modelu 'Crystal Plasticity' do programu Abaqus jest powszechnie używana do symulacji odkształcenia materiałów mono i bikrystalicznych. Niemniej jednak, w literaturze nie są dostępne stałe materiałowe dla tego modelu. W artykule zastosowano analizę odwrotną do pozyskania stałych materiałowych. Otrzymane parametry zostały wykorzystane i zweryfikowane w oparciu o dane doświadczalne ze ściskania bikryształów aluminium.

Received: November 29, 2010
Received in a revised form: December 23, 2010
Accepted: December 23, 2010